Journal of Materials Chemistry C

Accepted Manuscript

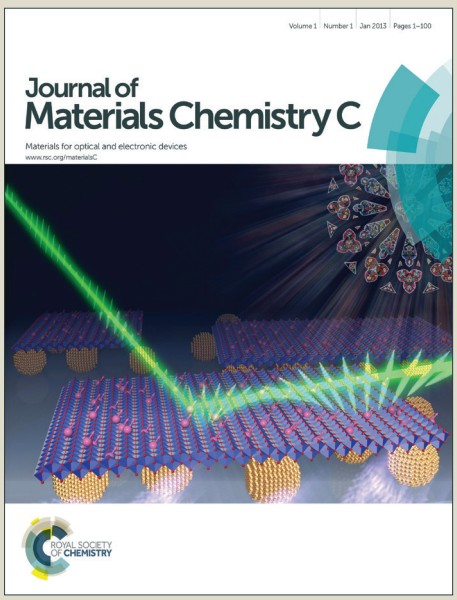

ROYAL SOCIETY OF CHEMISTRY

www.rsc.org/materialsC

Journal of
Materials Chemistry C

RSCPublishing

PAPER

Difunctional chemosensor for Cu(Ⅱ) and Zn (Ⅱ) based on Schiff base modified anthryl derivative with aggregation-induced emission enhancement and piezochromic characteristics

Mingdi Yang[a, b], Yan Zhang[a], Weiju Zhu[a], Huizhen Wang[a], Jing Huang[b], Longhuai Cheng[a], Hongping Zhou[a, *], Jieying Wu[a], Yupeng Tian[a]

Three new anthryl Schiff base derivatives containing similar molecular structure were synthesized through simple method and their fluorescent properties were investigated in detail. Among these, compound **1** displays aggregation-induced emission (AIE) feature, **2** exhibits aggregation-induced emission enhancement (AIEE) property, while **3** shows aggregation-caused quenching (ACQ) behavior. Single-crystal structure and theoretical calculation analysis show that the larger conjugation and the existence of multiple intra- and intermolecular interactions restrict the intramolecular vibration and rotation, which benifit the emission in the condensed state, while tightly dimer structure and intramolecular torsional motion induce fluorescence quenching. Moreover, compound **2** can be utilized as fluorescence on-off type sensor for Cu^{2+} in methanol/H_2O (4/1, v/v, pH 7.2) HEPES buffer solution, as well as fluorescence off-on type sensor for Zn^{2+} in pure methanol solution, respectively. The 2:1 ligand-to-metal coordiantion pattern of the **2**-Cu^{2+} and **2**-Zn^{2+} were calculated through Job's plot, and further comfirmed by X-ray crystal structures of complexes **2**-$CuBr_2$ and **2**-$ZnCl_2$. In addition, **2** also exhibits piezofluorochromic characteristic.

www.rsc.org/materialsC

Introduction

As the third and the second most abundant transition metal ions, Cu^{2+} and Zn^{2+} play vital roles in various biological processes, respectively, and their homeostasis are critical for the metabolism and development of living organism.[1] As a result, the development of selective chemosensors for Cu^{2+} and Zn^{2+} has raised widespread concerns, in particular, the fluorescent chemosensors due to the high selectivity, sensitivity, specificity, low detection limit and real-time monitoring with fast response of this type of sensors.[2] Up to now, a number of fluorescent chemosensors based on the signaling mechanisms of photoinduced electron transfer (PET),[3] fluorescence resonance energy transfer (FRET),[4] intramolecular charge transfer (ICT),[5] metal-ligand charge transfer (MLCT),[6] C=N isomerization,[7] aggregation-induced emission (AIE)[8] and metal-catalyzed reaction[9] have been developed and widely used. However, among these, relatively few chemosensors for both Cu^{2+} and Zn^{2+} have been reported.[10] Therefore, to develop chemosensors that can recognize multiple analytes remains a challenge.

Furthermore, most fluorescent compounds are trend to aggregation and become weakly emission or non-luminescent when dispersed in poor solvent or fabricated into films in the solid state. This notorious phenomenon is called "aggregation-caused quenching" (ACQ),[11] which greatly limits the applications as efficient fluorescent chemosensors.[12] During the last decade, materials with AIE or aggregation-induced enhanced emission (AIEE) properties have drawn much attention to provide an efficient approach to solve the problem of ACQ.[13] The AIE-active materials offer an unique platform for scientists to construct fluorescent sensors with high sensitivity and contrast, and so far, a lot of AIE-active fluorescent sensors have been developed.[14]

Anthryl derivatives were evidenced as excellent fluorophores and has been widely usded in the fluorescent sensors because of their excellent pthotoluminescence characteristics and chemical stabilities.[15] In this work, we synthesized three new Schiff base modified anthryl derivatives (**1-3**). Similar groups such as hydroxyphenyl, 4-diethylamino-2-hydroxypenyl and 4-diethylaminophenyl are adopted as terminal substituents, respectively. Their spectroscopic properties in solution and crystal state, the utility as fluorescent sensor and piezochromic luminescent material were investigated. The results showed that, **2** was proved to be as difunctional Cu^{2+} and Zn^{2+} fluorescent sensor, as well as piezochromic material with AIEE property. We aim to find how subtle changes on coordinating atoms, electron-withdrawing/donating property and steric hindrance modulate the AIE, recognition and piezochromic characteristics of these materials, and further reveal the struture-property relationship.

Experimental Section

Materials and apparatus

All of the reagents were obtained commercially and used as purchased. The chemical structures of these intermediates and target compounds were confirmed by IR, ^{1}H NMR, ^{13}C NMR and MALDI-TOF MS. IR spectra were recorded with an FT-IR spectrometer (KBr discs) in the 4000-400 cm^{-1} region. ^{1}H NMR and ^{13}C NMR spectra were recorded on a 400 MHz and 100MHz NMR instrument using DMSO-d_6 or CD_2Cl_2 as the solvent, respectively. Chemical shifts are reported in parts per million relative to internal TMS (0 ppm), and coupling constants are reported in hertz. Splitting patterns are described as singlet (s), doublet (d), triplet (t), quartet (q), or multiplet (m). Mass spectra were obtained on an autoflex speed MALDI-TOF mass spectrometer. Melting points were obtained on a Q2000 differential scanning calorimeter at a heating rate of 10 ^{o}C/min under nitrogen atmosphere. SEM images were obtained using a Hitachi S-4800 scanning electron microscope, and DLS measurements were conducted on a Delsa PNA54412AB Nano Submicron Grain Particle Size Analyzer. One-photon absorption spectra were recorded on a UV-265 spectrophotometer. One-photon-excited fluorescence spectra were measured using a Hitachi F-7000 fluorescence spectrophotometer. Powder X-ray diffraction experiments were operated on a Bruker D8 Advance powder X-ray diffractometer with Cu Kα radiation and a LyneEye detector.

Synthesis

Synthesis of 4-nitro-4'-(9-anthryl)-1, 2-stilbene (b). 2.4 g (21.6 mmol) *t*-BuOK and 4.0 g (8.8 mmol) **a** were placed into a dry mortar and well milled into powder, then 1.48 g (7.2 mmol) 9-anthracenecarboxaldehyde was added and mixed. The mixture was milled vigorously and monitored by thin-layer chromatography (TLC). The mixture became sticky and was continuously milled for another 1 h. After completion of the reaction, the mixture was dissolved in dichloromethane (DCM) and filtered, the filtrate was poured into H_2O and extracted by DCM. The organic phase was combined and dried over $MgSO_4$. After evaporation of the solvent, the crude product was recrystallized from ethanol, to give 1.38 g brown crystal. Yield: 58.9%. ^{1}H NMR: (DMSO-d_6, 400 MHz), δ (ppm): 7.17 (*d*, *J* = 16.0 Hz, 1H), 7.56-7.58(*m*, 4H), 8.10-8.15 (*m*, 4H), 8.31-8.36 (*m*, 4H), 8.44 (*d*, *J* =16.0 Hz, 1H), 8.63 (s, 1H); ^{13}C NMR (100 MHz, CD_3Cl, TMS, ppm): δ 147.2, 143.6, 135.1, 131.5, 131.3, 129.9, 129.7, 128.9, 127.5, 127.1, 126.0, 125.5, 125.4, 124.3; IR (KBr, cm^{-1}): 2975, 1602, 1578, 1554, 1522, 1403, 1348, 1269, 1181, 1149, 737 cm^{-1}; MALDI-TOF *m/z*: calcd for $[M]^+$, 325.1103; Found, 325.4047.

Synthesis of 4-amine-4'-(9-anthryl)-1, 2-stilbene (c). 2.0 g (6.2 mmol) **b** dissolved in 120 mL ethanol was added into a three-neck flask equipped with N_2 atmosphere and heated with a magnetic stirrer. Then 0.30 g of Pd/C catalyst was added into the preceding reaction system and the solution of 5 mL of 85% hydrazine was added dropwise for about 10 min. The reaction mixture was refluxed about 1.5 h and monitored by TLC. After the completion of the reaction, the reaction mixture was filtered under vacuum and recrystallized from ethanol to give the 1.20 g yellow needle crystal. Yield: 88.2%.^{1}H NMR: (DMSO-d_6, 400 MHz), δ (ppm): 5.39 (s, 2H), 6.65 (*d*, *J* = 8.0 Hz, 2H), 6.76 (*d*, *J* = 16.0 Hz, 1H), 7.48 (*d*, *J* = 8.0 Hz, 2H), 7.52 (*t*, *J* = 6.0 Hz, 4H), 7.75 (*d*, *J* = 16.0 Hz, 1H), 8.09 (t, *J* = 4.0 Hz, 2H), 8.34-8.36 (m, 2H), 8.50 (s, 1H) ; ^{13}C NMR (100 MHz, DMSO-d_6, TMS, ppm): δ 149.1, 137.7, 133.4, 131.1, 129.0, 128.5, 127.8, 125.8, 125.5, 125.4, 125.3, 124.7, 118.1, 113.8; IR (KBr, cm^{-1}): 3023, 1620, 1608, 1582, 1508, 1497, 1330, 1284, 1163, 734, 696, 537 cm^{-1}; MALDI-TOF *m/z*: calcd for $[M-H]^+$, 294.1361; Found, 293.7939.

Synthesis of 1. 2.1 g (7.2 mmol) **c** and 120 mL of methanol were added into a round-bottom flask equipped with a magnetic stirrer and heated at 70 ^{o}C for 10 min. A few drops of glacial acetic acid were then added to the preceding reaction system, and 1.2 g (9.8 mmol) of salicylaldehyde was added dropwise. The reaction mixture was refluxed for about 6 h and monitored by TLC. After the completion of the reaction, the reaction mixture was filtered under vacuum immediately to give 2.8 g of orange-yellow powder. Yield: 98.5%. m.p.: 204 ^{o}C. ^{1}H NMR: (DMSO-d_6, 400 MHz), δ (ppm): 6.99-7.05 (m, 3H), 7.45 (t, *J* = 8.0 Hz, 1H), 7.55 (d, *J* = 8.0 Hz, 6H), 7.71 (d, *J* = 8.0 Hz, 1H), 7.93 (d, *J* = 8.0 Hz, 2H), 8.12-8.14 (m, 2H), 8.19 (d, *J* = 16.0 Hz, 1H), 8.38 (d, *J* = 4.0 Hz, 2H), 8.59 (s, 1H), 9.03 (s, 1H), 13.19 (s, 1H); ^{13}C NMR (100 MHz, DMSO-d_6, TMS, ppm): δ 162.9, 162.4, 160.3, 138.7, 136.3, 135.8, 132.6, 132.3, 131.1, 129.0, 128.6, 127.9, 125.9, 125.7, 125.4, 124.7, 121.9, 119.4, 119.2, 116.6; IR (KBr, cm^{-1}): 3050, 2923, 2853, 1619, 1568, 1493, 1456, 1281, 1190, 1110, 759, 733 cm^{-1}; MALDI-TOF *m/z*: calcd for $[M + H]^+$, 400.1623; Found, 400.1329.

Synthesis of 2. Compound **2** was prepared according to a procedure similar to that for **1**, using 4-(diethylamino)salicylaldehyde (1.9 g, 9.8 mmol) instead of salicylaldehyde, to give 3.0 g of orange powder. Yield: 89.2%. m.p.: 230 ^{o}C. ^{1}H NMR: (DMSO-d_6, 400 MHz), δ (ppm): 1.14 (t, *J* = 6.0 Hz, 6H), 3.41-3.42 (m, 4H), 5.76 (s, 3H), 6.09 (s, 1H), 6.99 (d, *J* = 16.0 Hz, 1H), 7.38 (d, *J* = 12.0 Hz, 1H), 7.43 (d, *J* = 8.0 Hz, 2H), 7.54-7.56 (m, 4H), 7.87 (d, *J* = 4.0 Hz, 2H), 8.11-8.15 (m, 3H), 8.36-8.38 (m, 2H), 8.58 (s, 1H), 8.81 (s, 1H); ^{13}C NMR (100 MHz, DMSO-d_6, TMS, ppm): δ 161.3, 160.9, 152.4, 137.2, 135.1, 134.3, 132.0, 130.1, 129.0, 128.0, 126.8, 126.4, 125.9, 125.6, 124.5, 121.6, 109.4, 104.3, 97.8, 46.0, 12.9; IR (KBr, cm^{-1}): 2972, 1624, 1576, 1519, 1350, 1242, 1201, 1132, 827, 735 cm^{-1}; MALDI-TOF *m/z*: calcd for $[M]^+$, 470.2358; Found, 470.4244.

Synthesis of 3. Compound **3** was prepared according to a procedure similar to that for **1**, using 4-diethylaminobenzaldehyde (1.2 g, 9.8 mmol) instead of salicylaldehyde, to give 3.2 g of orange powder. Yield: 90.6%. m.p.: 223 ^{o}C. ^{1}H NMR: (DMSO-d_6, 400 MHz), δ (ppm): 1.13-1.16 (m, 6H), 3.43-3.45 (m, 4H), 6.77 (d, *J* = 8.0 Hz, 2H), 6.98 (d, *J* = 16.0 Hz, 1H), 7.29 (d, *J* = 8.0 Hz, 2H), 7.54-7.56 (m, 4H), 7.76 (d, *J* = 8.0 Hz, 2H), 7.82 (d, *J* = 8.0 Hz, 2H), 8.07-8.13 (m, 3H), 8.36-8.39 (m, 2H), 8.48 (s, 1H), 8.57 (s, 1H); ^{13}C NMR (100 MHz, CD_2Cl_2, TMS, ppm): δ 164.6, 159.9, 144.0, 137.4, 133.4, 132.0, 131.2, 130.1, 129.0, 127.9, 127.8, 126.6, 126.4, 125.8, 125.6, 121.7, 120.5, 111.4, 106.9, 44.9, 12.7; IR (KBr, cm^{-1}): 3024, 1584, 1488, 1331, 1288, 1166, 888, 733, 697, 533 cm^{-1}; MALDI-TOF *m/z*: calcd for $[M - H]^+$, 453.2409; Found, 453.9600.

X-ray Crystallography

The X-ray diffraction measurements were performed on a Bruker Smart 1000 CCD area detector using graphite monochromated MoKα radiation (λ = 0.71069 Å). Intensity data were collected in the variable ω-scan mode. The structures were solved by direct methods and difference Fourier syntheses. Non-hydrogen atoms were refined anisotropically, and hydrogen atoms were introduced geometrically. Calculations were performed with SHELXTL-97[16] program package. The processing parameters for five compounds are shown in **Table 1**.

Table 1. Crystallographic data for **1-3, 2**-$CuBr_2$ **and 2**-$ZnCl_2$.

compound	**1**	**2**	**3**
empirical formula	$C_{29}H_{21}NO$	$C_{67}H_{62}Cl_2N_4O_2$	$C_{33}H_{30}N_2$
formula weight	399.47	1026.11	454.59
crystal system	Monoclinic	Monoclinic	Monoclinic
space group	*P*2(1)/c	*P*2(1)/n	*P*2(1)/n
a [Å]	24.405(18)	11.001(4)	13740(5)
b [Å]	7.319(5)	12.498(5)	12.487(5)
c [Å]	11.824(9)	19.746(8)	15.071(5)
β[°]	101.249(5)	94.205(5)	100.349(5)
V [Å^3]	2071.4(17)	2707.6(18)	2543.7(16)
Z	4	2	4
T [K]	298(2)	298(2)	298(2)
Dcalcd[g ·cm-3]	1.281	1.259	1.187
μ [mm-1]	0.077	0.171	0.069
*θ*range [°]	0.85-25.00	1.93-25.00	1.85-25.00
total no. data	13955	18899	17873
no.unique data	3654	4750	4468
no. params refined	281	355	318
R_1	0.0420	0.0580	0.0577
wR_2	0.1527	0.1932	0.1736
GOF	1.082	1.011	1.029

compound	**2**-$CuBr_2$	**2**-$ZnCl_2$
empirical formula	$C_{67}H_{62}Br_2N_4O_3Cu$	$C_{67}H_{60}Cl_2N_4O_3Zn$
formula weight	1194.57	1105.46
crystal system	Triclinic	Triclinic
space group	P-1	P-1
a [Å]	10.4540(19)	10.4906(16)
b [Å]	15.812(3)	15.644(2)
c [Å]	18.477(3)	18.204(3)
α[°]	90.856(2)	90.239(2)
β[°]	91.576(2)	90.327(2)
γ[°]	96.166(2)	95.162(2)
V [Å^3]	3035.1(10)	2975.3(8)
Z	2	2
T [K]	296(2)	296(2)
Dcalcd[g ·cm-3]	1.307	1.234
μ [mm-1]	1.724	0.551
*θ*range [°]	1.10-25.60	1.12-25.50
total no. data	22570	65277
no.unique data	11236	10899
no. params refined	717	718
R_1	0.0616	0.0864
wR_2	0.1719	0.2059
GOF	1.107	1.084

Results and discussion

Synthesis

Scheme 1 shows the synthesis routes of three compounds. Intermediate (4-nitrobenzyl)triphenylphosphine bromide (**a**) was synthesized efficiently according to the literature methods previously published.[17] All of the compounds were easily obtained from aldehydes in high yields *via* nucleophilic addition reactions with intermediate **c**. The detailed procedures for the intermediates and final products data are described in the experimental section and supporting information (**Fig. S11-S23**).

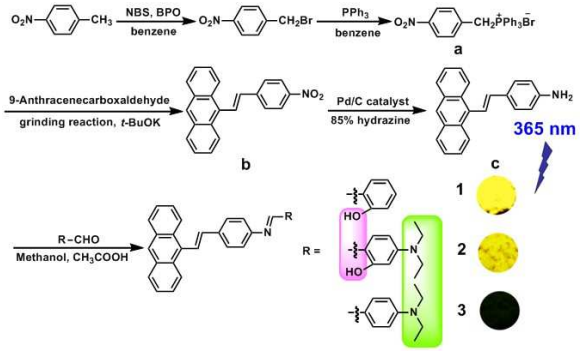

Scheme 1 Synthetic routes to target compounds **1-3**.

Photophysical Properties

The normalized one-photon absorption and photoluminescence (PL) spectra of compounds **1-3** in acetonitrile solution at a concentration of 10 μM are shown in **Fig. 1**. The absorption maximum of compounds **1-3** located at 387, 406 and 401 nm, respectively, which can be assigned to the π-π* transitions and intramolecular charge transfer (ICT) processes (**Fig. 2**).[18] Comparing the maxima absorption wavelength of these compounds, it's clear that, the absorption spectra show obvious red-shift with the extension of the π-systems and the strong electron donating ability. As for the fluorescence emission, the intensity of **2** solution is much stronger than those of others under the same measurement condition.

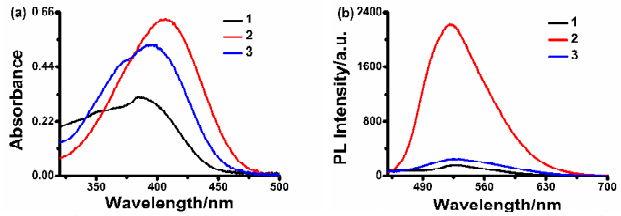

Fig. 1 Absorption and fluorescent spectra of **1-3** (10 μM) in acetonitrile solution.

To better understand the relationship between the photophysical properties and the electronic structures, we performed the quantum mechanical computations with TD-DFT/B3LYP/6-31G Gaussian method to obtain the lowest energy spatial conformation of the compounds **1-3** in the ground state.[19] The highest occupied molecular orbitals (HOMOs) and the lowest unoccupied molecular orbitals (LUMOs) plots of compounds **1-3** are given in **Fig. 2**. The dihedral angles of **1-3** in gas phase (generally, the molecular geometry in dilute solution can be represented by that of the gas phase) shown in **Table S2**. We can see molecules **1** and **3** adapt twisted conformations, thus contributing little to the energy levels of the luminogen. By contrast, the molecule **2** assumes a planar conformation at the terminal aromatic ring, which results in an enlarged conjugation, thus the enhanced emission of **2** in solution. The calculated energy band gaps for compounds **1-3** are 3.24, 3.07 and 3.35 eV, respectively. The trend is the same as that of the experimental data. The theoretical study nicely explains the photophysical properties of compounds **1-3**.

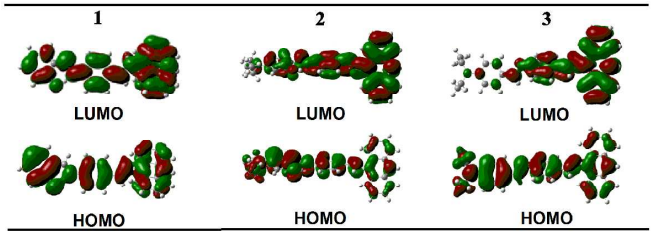

Fig. 2 Electron density distribution of frontier molecular orbitals of **1-3**.

Aggregation-Induced Emission Properties

To further study the optical behavior of the aggregation process of these compounds, a solvent-poor solvent absorption and fluorescence tests were performed. Acetonitrile was used as the good solvent and methanol was used as the poor solvent. The concentration was maintained at 10 μM. As shown in **Fig. 3b**, compound **2** displays a middle PL intensity in pure acetonitrile solution, and the PL intensity is gradually intensified with gradual addition of methanol to the acetonitrile. From the pure acetonitrile solution to acetonitrile/methanol mixture with methanol fraction of 90%, the PL intensity increases by 3.63-fold, showing the characteristic of AIEE. At the same time, a maximum fluorescence quantum yields (Φ_F) of 29.5% was recorded. Furthermore, with gradual addition of methanol to the acetonitrile solution, the maximum emission wavelength of **2** shows blue shifted of 10 nm. One possible reason for this change can be explained as reported in the literature: when poor solvent methanol was added, **2** molecules start to aggregate, resulting in less polar microenvironment for the luminogens due to self-wrapping. The microenvironment gets less and less polarity with more serious aggregation caused by increased methanol fraction, thus reversely giving blue shifted emissions.[20] However, there is another possible reason that the multiple intramolecular N···O interactions formed by *o*-hydroxyl group on the terminal benzene ring would be broken with the addition of methanol, which could also lead to blue shift. The absorption bands of **2** in the acetonitrile/methanol mixtures are very similar to its absorption in dilute acetonitrile solutions, as shown in **Fig. 3a**. Meanwhile, the obvious leveling-off tails in the long-wavelength region are caused by the Mie effect of the particle suspension.[21] What's interesting is, with the addition of methanol, the emissions of **1** enhance slowly, the PL intensity only increases by 0.38-fold (**Fig. S2**), however, in the solid, compound **1** emit bright yellowish-orange light (Scheme 1), and the Φ_F is 15.4%, which shows obvious AIE property. This phenomenon might be related to the presence intermolecular interaction formed between *o*-hydroxyl group on the terminal benzene ring of compound **1** and methanol. As far as compound **3**, the emissions declined gradually with the addition of methanol (**Fig. S2**), namely, compound **3** has the feature of ACQ.

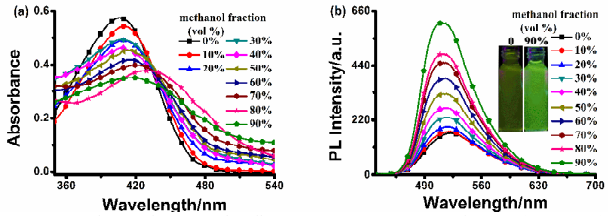

Fig. 3 Absorption and fluorescent spectra of **2** (10 μM) in acetonitrile/methanol mixtures with different methanol fractions. The inset depicts the changes of PL peak intensity with different methanol fractions.

In order to determine whether compound **2** can form nanostructures and the dimensions of the nano-aggregates formed, the growth progresses of **2** was studied by scanning electron microscopy (SEM) and dynamic light scattering (DLS) with high methanol content. As can be seen in **Fig. 4**, with the increasing proportion of methanol, nanoparticles emerged immediately and separately dispersed, and the size of the particles became smaller, which is in good agreement with DLS data. **Fig. 4** also reveals the existence of particles with average size of 560 nm in the acetonitrile/methanol mixture with 70% methanol fraction. The size of the aggregates decreased to 188 nm after methanol fraction increases to 90%, respectively.

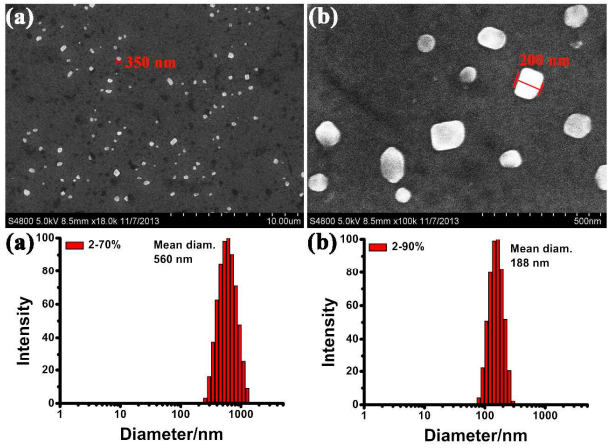

Fig. 4 SEM images and particle size distributions of **2** in acetonitrile/methanol mixtures with different methanol fractions: (a) **2** in acetonitrile/methanol (30/70, v/v); (b) **2** in acetonitrile/methanol (10/90, v/v).

Crystal structure

Crystal structure is important for us to understand the optoelectronic properties and molecular packing. Single crystals of compounds **1-3** were obtained by slow evaporation from the solutions in DCM/methanol or DCM/acetonitrile mixtures at room temperature. Their crystal data are summarized in **Table 1**. Some of the packing interactions in the crystals are depicted in **Fig. 5-7**. As shown in **Table 1**, compounds **1-3** all crystallize in the monoclinic system (space group *P*2(1)/c for **1**, space group *P*2(1)/n for **2** and **3**). For compounds **1-3**, each unit cell contains one compound molecule, in addition, there is one DCM molecule in the unit cell of **2**. The dihedral angles between terminal aromatic ring (P_1) and benzene ring plane (P_2), P_2 and anthracene ring (P_3) are 1.79°, 65.29° for **1**, 35.58°, 66.71° for **2** and 44.83°, 79.63° for **3**. Figures **5-7** show that **1-3** molecules all have several kinds of weak intra- and intermolecular interactions, and partial data are given in **Table S2**.

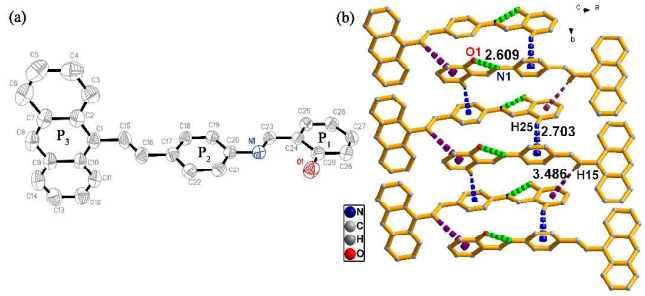

Fig. 5 (a) ORTEP diagram of **1**; (b) View of a 1D chain of **1** showing the C-H···π (blue and violet) hydrogen bond and N···O (green) bond along the *b*-axis. Hydrogen atoms except H15 and H25 are omitted for clarity.

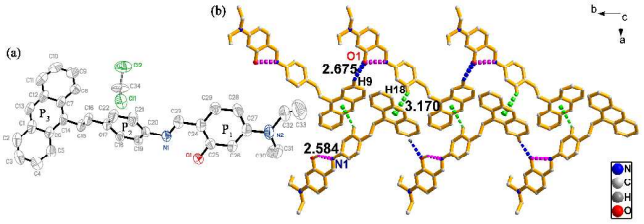

Fig. 6 (a) ORTEP diagram of **2**; (b) View of a 1D chain of **2** showing the C-H···π (green) hydrogen bond, C-H···O (blue) hydrogen bond and N···O (pink) bond along the *b*-axis. Hydrogen atoms except H9 and H18 are omitted for clarity.

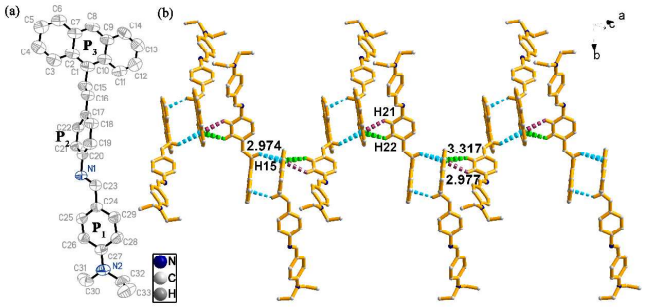

Fig. 7 (a) ORTEP diagram of **3**; (b) View of a 1D chain of **3** showing the C-H···π (lightcyan, green and violet) hydrogen bond along the *a*-axis. Hydrogen atoms except H15, H21 and H22 are omitted for clarity.

Compounds **1** and **2** both have an *o*-hydroxyl group on the terminal benzene ring and form multiple intramolecular N···O interactions (d = 2.609 Å for **1** and 2.584 Å for **2**). As shown in **Fig. 5b**, **1** has only the 1D layer structure, pairs of molecules are also bound together through two kinds of C-H···π hydrogen bond (d = 2.703 Å and 3.486 Å) to form dimers in the ground state. For **2** (**Fig. 6b**), because of the steric hindrance of the N, N-diethylamino group on terminal benzene ring and the roles of the intermolecular hydrogen bonds, the dihedral angle between P_1 and P_2 (35.58°) is more distorted than molecule **1** (1.79°). Three adjacent molecules form a ring of trimer structure through two kinds of intermolecular hydrogen bonds (d = 2.675 Å and 3.170 Å) in the crystal. Compounds **1** and **2** displayed different fluorescence behaviors in various states. For **1**, the relatively planar geometry (1.79° for P_1-P_2) caused by intramolecular hydrogen bond enables the larger conjugation, which may be beneficial to emission in solid. Nevertheless, in the acetonitrile/methanol mixed solution, these intramolecular hydrogen bonds might be destroyed by the methanol molecules, reduce conjugation and ultimately lead to fluorescence quenching. On the contrary, for **2**, large conjugation enhances emission in the solution and multiple intra-/intermolecular interactions rigidify the conformation which would be helpful to emission in the solid. As for **3**, doesn't contain *o*-hydroxyl group on the terminal benzene ring, there are only three kinds of intermolecular hydrogen bonds (d = 2.974 Å, 2.977 Å and 3.317 Å). Among them, anthracene ring on the two adjacent molecules linked together through C-H···π hydrogen bond (2.974 Å) to form particular dimers (**Fig. 7b**). By contrast, these three hydrogen bonds are all located in the side of anthracene ring, and there is no force on the terminal group of 4-diethylaminophenyl. As a result, the excited-state energy is consumed by intramolecular rotation motion, thus enabling the molecules to emit hardly in the concentrated state.

Uv-vis and fluorogenic Cu^{2+} sensing

The sensor properties of these anthryl-substituted Schiff bases were evaluated in the methanol/H_2O (4/1, v/v, pH 7.2) HEPES buffer solution. The photophysical properties of three compounds with several metal cations (solutions of Hg^{2+}, Mn^{2+} and Zn^{2+} were prepared from their chloride salts; solutions of Ag^{+}, Al^{3+}, Ba^{2+}, Ca^{2+}, Cd^{2+}, Co^{2+}, Cr^{3+}, Cu^{2+}, Fe^{3+}, K^{+}, La^{3+}, Li^{+}, Mg^{2+}, Na^{+}, Ni^{2+} and Pb^{2+} were prepared from their nitrate salts) were investigated by UV-vis absorption and fluorescence measurements.[22] As shown in **Fig. 8a**, the absorbance centered at 432 nm remained unchanged on addition of several kinds of metal ions except in the case of Cu^{2+}. Upon addition of Cu^{2+}, the absorbance located at 432 nm was decreased and blue shifted to 408 nm. And the fluorescence spectra of **2** also has a special response to Cu^{2+}, namely, the emission intensity is weakened (*ca.* 0.09 times of **2**) (**Fig. 8b**). However, no remarkable changes of fluorescence intensity of **1** and **3** have been observed (**Fig. S3**). The selectivity toward Cu^{2+} was further ascertained by the competition experiments. As shown in **Fig. 9**, the PL intensity of **2** in the presence of Cu^{2+} (1 equiv.) are almost unaffected by the addition of most competing metal ions.

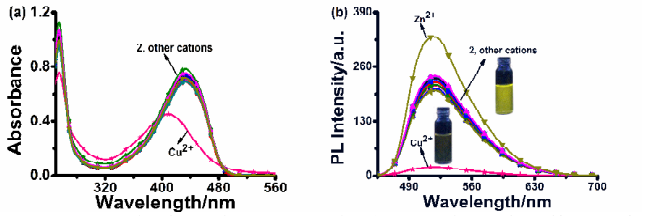

Fig. 8 (a) UV-vis absorption spectra of **2** (10 μM) in methanol/H_2O (4/1, v/v, pH 7.2) HEPES buffer solution with 1 equiv. different metal ions. (b) Fluorescent spectra of **2** (10 μM) in methanol/H_2O (4/1, v/v, pH 7.2) HEPES buffer solution with 1 equiv. different metal ions.

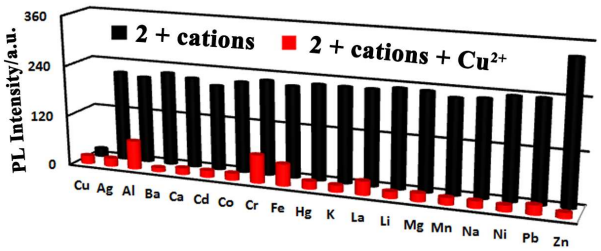

Fig. 9 Fluorescence intensity change of **2** (10 μM) with Cu^{2+} (10 μM) in methanol/H_2O (4/1, v/v, pH 7.2) HEPES buffer solution in the presence of competing metal ions (10 μM).

To elicit the interactions between compound **2** and Cu^{2+}, UV-vis and fluorescence spectra variation of **2** (10 μM) in methanol/H_2O (4/1, v/v, pH 7.2) HEPES buffer solution was titrated with Cu^{2+} from 0 to 16 μM at room temperature. As shown in **Fig. 10a**, three isosbestic points were observed at 290, 392 and 491 nm when spectra were recorded with varying concentrations of Cu^{2+}, accordingly, the PL intensity was decreased progressively (**Fig. 10b**). Therefore, compound **2** can be utilized as a selective on-off type fluorescence sensor for Cu^{2+}. By plotting the absorbance and PL intensity changes as a function of concentration the detection limits of **2**-Cu^{2+} were calculated to be about 5.53×10^{-7} M and 2.12×10^{-7} M based on the DL = $3\sigma/K$ (σ is the standard deviation of blank measurements, and K is the slop between the absorbance or fluorescence versus Cu^{2+} concentration, **Fig. S4**), respectively.[23] Job's plot analysis based on the method of continuous variation was carried out in mixed solution revealed a 2:1 ligand-to-metal binding mode (**Fig. 11**). On the basis of 2:1 stoichiometery, the association constant between **2** and Cu^{2+} was estimated to be 1.16×10^{8} M^{-1} and 1.28×10^{8} M^{-1} by using the Benesi-Hilderbrand equation (**Fig. S5**), respectively.[24]

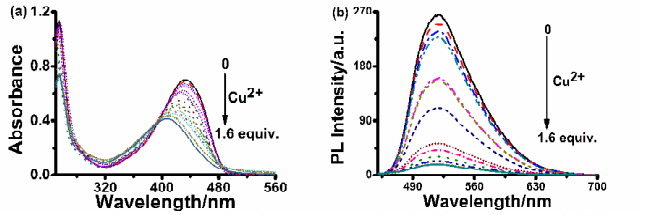

Fig. 10 (a) Fluorescence titration spectra of **2** in the presence of different concentration of Cu^{2+} (0-1.6 equiv.) in methanol/H_2O (4/1, v/v, pH 7.2) HEPES buffer solution; (b) Normalized response of fluorescence signal of **2** in the prescence of different concentration Cu^{2+} .

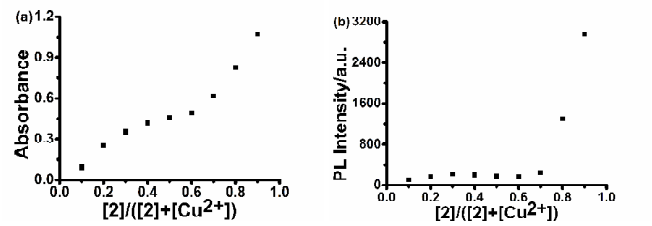

Fig. 11 Job's plot of **2** and Cu^{2+} in methanol/H_2O (4/1, v/v, pH 7.2) HEPES buffer solution. The total concentration of **2** and Cu^{2+} was 10 μM. (a) Absorbance at 520 nm. (b) Fluorescence intensity at 508 nm.

Subsequently, the acid-base titration experiment revealed that **2** dose not show significant fluorescence changes within the pH range 7 to 12 (**Fig. S6**), which indicates that compound **2** can be employed for the detection of Cu^{2+} in neutral pH range (pH 7.2). Since many sensor response are affected by the presence of anions, the fluorescence response of **2** toward Cu^{2+} in the presence of various commonly coexistent anions such as Cl^-, Br^-, SO_4^{2-} and AcO^- also was investigated (**Fig. S7**). The results show that all the tested anions have no influence on the compound **2**. In addition, the reversibility of the metal complexation process is tested by adding Na_2S (10 μM) to the solution of **2**-Cu^{2+} (**Fig. S8**). The result demonstrates that compound **2** could be easily regenerated for repeating use. And the result also indicates that the binding of **2** to Cu^{2+} is a chemically reversible coordination rather than a metal cation-catalyzed reaction.

Fluorogenic Zn^{2+} sensing

In addition, for compound **2**, it also shows excellent selectivity on Zn^{2+} in the pure methanol solution. As depicted in **Fig. 12**, the PL intensity of **2** increased remarkably (*ca.* 4.4 times of **2**) with slightly blue shift (*ca.* 10 nm). The results of competition experiment indicated that, the fluorescence intensity of **2** in the presence of Zn^{2+} (1 equiv.) are unaffected by the addition of most competing metal ions. However, Al^{3+}, Cr^{3+}, Cu^{2+} and Fe^{3+} showed fluorescence quenching after they were added to **2**, which could be the strongly chelation activity with **2** (**Fig. S9**). Moreover, the fluorescence response of **2** to $Zn(NO_3)_2$, $ZnCl_2$, $ZnBr_2$, ZnI_2, $ZnSO_4$, ZnSCN and $Zn(OAc)_2$ gave the similar results. As shown in **Fig. S10**, no significant changes was observed, which indicated that the counter ions didn't affect the detection of Zn^{2+}.

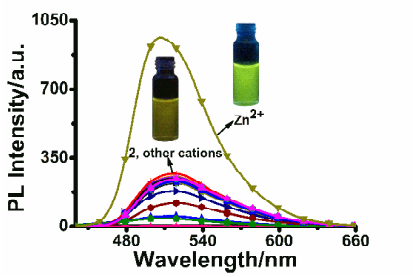

Fig. 12 Fluorescent spectra of **2** (10 μM) in methanol solution with 1 equiv. different metal ions.

The gradual changes of the fluorescence spectra of **2** (10 μM) upon addition of Zn^{2+} (0-20 μM) are shown in **Fig. 13a**, obviously, compound **2** also can be utilized as an off-on type fluorescence sensor for Zn^{2+}. The results of Job's plot experiment showing a 2:1 stoichiometry complexation between **2** and Zn^{2+} (**Fig. 14a**). Accordingly, the detection limits and the association constant of **2**-Zn^{2+} were calculated to be 7.19×10^{-8} M and 1.05×10^{6} M^{-1} (**Fig. 13b**, **14b**), respectively.

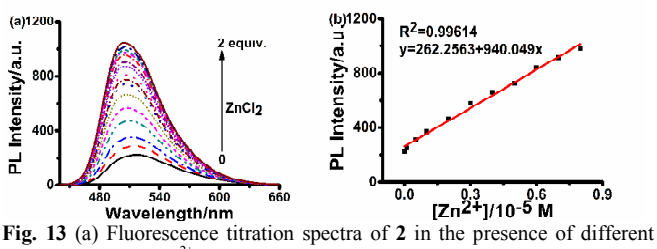

Fig. 13 (a) Fluorescence titration spectra of **2** in the presence of different concentration of Zn^{2+} (0-2 equiv.) in methanol solution; (b) Normalized response of fluorescence signal of **2** in the prescence of different concentration Zn^{2+}.

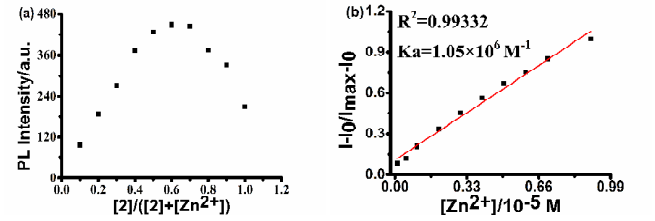

Fig. 14 (a) Job's plot of **2** and Zn^{2+} in methanol solution. The total concentration of **2** and Zn^{2+} was 10 μM; (b) Fluorescence intensity ration ($I-I_0/I_{max}-I_0$) as the square of Zn^{2+} concentration.

Coordination mode of 2 to Cu^{2+} and Zn^{2+}

The single crystal structures of complexes **2**-$CuBr_2$ and **2**-$ZnCl_2$ explained the coordination mode well (**Fig. 15**). Both complexes crystallize in a triclinic system with space group P-1 (**Table 1**). And it was clear that two molecules of **2** are present in the asymmetric unit along with one molecule of $CuBr_2$ or $ZnCl_2$, and a 2:1 species are formed between **2** and $CuBr_2$ (or $ZnCl_2$) through oxygen atom of hydroxyl, then to form a four-coordinated, tetrahedral geometry. Obviously, both complexes employed the same 2:1 ligand-to-metal coordiantion pattern, which consistent with the results of Job's plot.

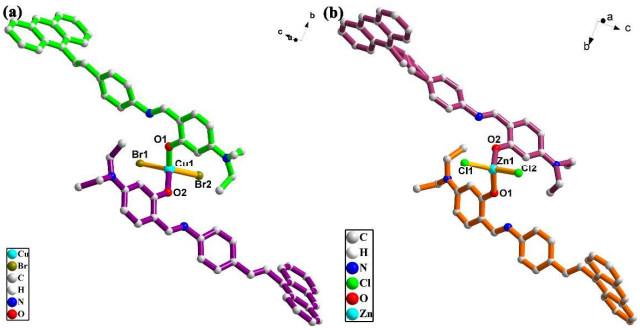

Fig. 15 X-ray crystal structures of complexes **2**-$CuBr_2$ (a) and **2**-$ZnCl_2$ (b).

According to the single crystal structures of complex **2**-$CuBr_2$ and **2**-$ZnCl_2$, the most likely coordination mode are depicted in **Scheme 2**. Although the same coordiantion pattern can be found in the crystal structures, the fluorescence properties are completely different. This could be due to the different metal ions' electronic configuration. For Zn^{2+}, there have filled core-like d-orbitals and thus no d-d transitions are possible, which would be likely to lead to enhanced fluorescence.[25] As far as Cu^{2+}, the d^9 electronic configuration played an important role in the control process of photoinduced electron transfer (PET) process and caused fluorescence quenching.[26]

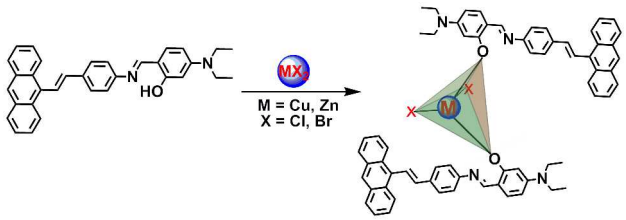

Scheme 2. Proposed binding mode of **2** with Cu^{2+} and Zn^{2+}.

Solid state piezochromic luminescence

The piezofluorochromic (PFC) materials with tunable light-emitting behaviors have attracted much interest due to their potential applications as sensors, memories, security inks, logicgate units, etc.[27] In this case, we examined the PFC behavior of solid compound **2** by grinding with a mortar and pestle. As shown in **Fig. 16a**, the pristine orange solid **2** emits yellowish-orange fluorescence. However, when it is ground, compound changed into yellow-emitting under ambient light and 365 nm UV light. The PL emission peak after grinding is located at 523 nm, which is 15 nm blue-shifted from the spectrum of the solid powder before grinding. The blue shift observed in the ground solid powder may be attributable to conformation planarity in the molecular packing process, during which the **2** molecules may adjust themselves by destroying the intermolecular interactions. Without such restraint, the molecules may assume a twisted conformation, which destroys the conjugation, and hence results in a blue-shifted emission.

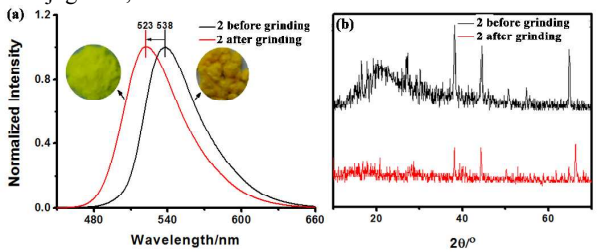

Fig. 16 Fluorescence spectra and images (a) as well as WXRD curves (b) of **2** before and after grinding.

To gain further insight into the mechanism for the PFC, we carried out wide-angle X-ray diffraction (WXRD) measurements for compound **2** before and after grinding treatment. According to the WXRD measurements (**Fig. 16b**), the diffraction curve of the original sample exhibits numerous sharp and intense diffraction peaks, indicative of its crystalline nature. In contrast, the ground sample is amorphous as its diffractograms exhibit a weak, broad and diffuse peak, indicating that the ordered structure has been destroyed after grinding. The result shows that the structural changes in the mode of molecular packing under external grinding can induce a significant PFC property.

Conclusions

In summary, three different aggregation fluoresence behaviors of anthryl Schiff bases **1-3** were synthesized and optical, sensory as well as piezochromic properties were investigated. Among them, compound **2** shows strong affinity for Cu^{2+} and Zn^{2+} over other cations such as Ag^{+}, Al^{3+}, Ba^{2+}, Ca^{2+}, Cd^{2+}, Co^{2+}, Cr^{3+}, Fe^{3+}, Hg^{2+}, K^{+}, La^{3+}, Li^{+}, Mg^{2+}, Mn^{2+}, Na^{+}, Ni^{2+} and Pb^{2+} in methanol/H_2O (4/1, v/v, pH 7.2) HEPES buffer solution and in pure methanol solution, respectively. Single crystal structures of complexes **2**-$CuBr_2$ and **2**-$ZnCl_2$ explain well the 2:1 binding mode between ligand and metal ions. Further experiments indicate that the fluorescent signals of **2** can be restored by the addition of Na_2S in to **2**-Cu solutions. In addition, compound **1** displays AIE feature, **2** shows AIEE property and **3** exhibits ACQ behavior. And compound **2** can also be utilized in optical recording and pressure sensing fields due to its excellent structural changes before and after grinding. Comprehensive analysis showed that 4-diethylamino and *o*-hydroxyl groups on the terminal benzene ring play an important role on the molecular structure and performance. On the one hand, 4-diethylamino has large steric hindered and strong electron donor ability. On the other hand, *o*-hydroxyl group is easy to form intramolecular N···O interaction and the larger conjugation extent of molecule. Moreover, compared with our previous study,[28] substituted flat anthryl with weak electron-donating ability in place of distorted triphenylamine (TPA) unit, there are also some great differences on molecular properties. Above results demonstrate that the combined effects of various functional groups have a great influence on molecular structure and performance.

Acknowledgment

This work was supported by the Program for New Century Excellent Talents in University (China), the Doctoral Program Foundation of the Ministry of Education of China (20113401110004), the National Natural Science Foundation of China (21271003, 21271004, 51432001 and 51472002), the Ministry of Education, the Natural Science Foundation of Education Committee of Anhui Province (KJ2012A024), the Natural Science Foundation of Anhui Province (1408085QB26), the 211 Project of Anhui University, Higher Education Revitalization Plan Talent Project of (2013), the Opening Project of the Key Laboratory of Opt-electronic Information Acquistion and Manipulation Ministry of Education (OEIAM 201402).

Notes and References

[a]*Key Laboratory of Opto-Electronic Information Acquisition and Manipulation, Ministry of Education, College of Chemistry and Chemical Engineering, Anhui University, Hefei, 230601, P. R. China.*
[b]*School of Materials and Chemical Engineering, Anhui Jianzhu University, Hefei, 230601, P. R. China.*
**Corresponding author. Fax: +86-551-63861279, Tel: +86-551-63861279.*

Crystallographic data have been deposited with the Cambridge Crystallographic Data Centre as supplementary publication no. CCDC: 971199, 942451, 971201, 1030694 and 1031321.
Electronic Supplementary Information (ESI) available: **Fig.S1-S23**, **Tables S1-S2**.

1 (a) H. Tapiero, D. M. Townsend, K. D. Tew, *Biomed. Pharmacother.* 2003, **57**, 386; (b) E. Gaggelli, H. Kozlowski, D. Valensin, G. Valensin, *Chem. Rev*. 2006, **106**, 1995; (c) M. P. Cuajungco, K. Y. Faget, *Brain Res. Rev*. 2003, **41**, 44; (d) J. M. Berg, Y. Shi, *Science*, 1996, **271**, 1081.
2 (a) Q. Zhao, F. Li, C. Huang, *Chem. Soc. Rev.* 2010, **39**, 3007; (b) D. W. Domaille, L, Zeng, C. J. Chang, *J. Am. Chem. Soc*. 2010, **132**, 1194; (c) Y. Zhou, F. Wang, Y. Kim, S. Kim, J. Yoon, *Org. Lett*. 2009, **11**, 4442; (d) M. A. Palacious, Z. Wang, V. A. Montes, G. V. Zyryanov, Jr, P. Anzenbacher, *J. Am. Chem. Soc*. 2008, **130**, 10307; (e) L. Xue, C. Liu, H. Jiang, *Chem. Commun*. 2009, 1061.
3 (a) T. Y. Liu, X. G. Liu, D. R. Spring, X. H. Qian, J. N. Cui, Z. C. Xu, *Scientific Reports* 2014, **4**, 5418; (b) P. Ashokkumar, V. T. Ramakrishnan, P. Ramamurthy, *J. Phys. Chem. A* 2011, **115**, 14292; (C) S. L. Liu, D. Li, Z. Zhang, G. K. S. Prakash, P. S. Conti, Z. B. Li, *Chem. Commun*. 2014, **50**, 7371.
4 (a) A. Sahana, A. Banerjee, S. Lohar, B. Sarkar, S. K. Mukhopadhyay, D. Das, *Inorg. Chem*. 2013, **52**, 3627; (b) L. L. Long, W. Y. Lin, B. B.

Chen, W. S. Gao, L. Yuan, *Chem. Commun*. 2011, **47**, 893; (c) Z. J. Hu, J. W. Hu, Y. Cui, G. N. Wang, X. J. Zhang, K. Uvdal, H. W. Gao, *J. Mater. Chem. B* 2014, **2**. 4467.

5 (a) F. B. Yu, P. Li, P. Song, B. S. Wang, J. Z. Zhao, K. L. Han, *Chem. Commun*. 2012, **48**, 2852; (b) X. Q. Chen, Y. Zhou, X. J. Peng, J. Y. Yoon, *Chem. Soc. Rev*. 2010, **39**, 2120.

6 (a) B. K. An, S. K. Kwon, S. D. Jung, S. Y. Park, *J. Am. Chem. Soc.*, 2002, **124**, 14410-14415; (b) S. K. Chung, Y. R. Tseng, C. Y. Chen, S. S. Sun, *Inorg. Chem*. 2011, **50**, 2711.

7 (a) Y. Q. Sun, P. Wang, J. Liu, J. Y. Zhang, W. Guo, *Analyst* 2012, **137** 3430; (b) P. Wang, J. Liu, X. Lv, Y. L. Liu, Y. Zhao, W. Guo, *Org. Lett*. 2012, **14**, 520; (c) H. S. Jung, K. C. Ko, J. H. Lee, S. H. Kim, S. Bhuniya, J. Y. Lee, Y. Kim, S. J. Kim, J. S. Kim, *Inorg. Chem.* 2010, **49**, 8552.

8 (a) J. S. Wu, W. M. Liu, J. C. Ge, H. Y. Zhang, P. F. Wang, *Chem. Soc. Rev*. 2011, **40**, 3483; (b) J. Mei, Y. J. Wang, J. Q. Tong, J. Wang, A. J. Qin, J. Z. Sun, B. Z. Tang, *Chem. Eur. J*. 2013, **19**, 613; (c) T. Noguchi, A. Dawn, D. Yoshihara, Y. Tsuchiya, T. Yamamoto, S. Shinkai, *Macromol. Rapid Commun*. 2013. **34**. 779.

9 (a) L. Xu, Y. F. Xu, W. P. Zhu, B. B. Zeng, C. M. Yang, B. Wu, X. H. Qian, *Org. Biomol. Chem*. 2011, **9**, 8284; (b) Z. X. Li, L. F. Zhang, L. N. Wang, Y. K. Guo, L. H. Cai, M. M. Yu, L. H. Wei, *Chem. Commun*. 2011, **47**, 5798; (c) M. M .Yu, Z. X. Li, L. H. Wei, D. H. Wei, M. S. Tang, *Org. Lett*. 2008, **10**, 5115.

10 (a) L. M. Hyman, K. J. Franz, *Coord. Chem. Rev*. 2012, **256**, 2333; (b) X. Chen, S. W. Nam, M. J. Jou, Y. Kim, S. J. Kim, S. Park, J. Yoon, *Org. Lett*. 2008, **10**, 5235; (c) M. D. Yang, H. Z. Wang, J. Huang, M. Fang, B. Mei, H. P. Zhou, J. Y. Wu, Y. P. Tian, *Sens. Actuators B* 2014, **204**, 710.

11 (a) R. H. Friend, R. W. Gymer, A. B. Holmes, J. H. Burroughes, R. N. Marks, C. Taliani, *Nature* 1999, **397**, 121; (b) T. P. I. Saragi, T. Spehr, A. Siebert, T. Fuhrmann-Lieker, J. Salbeck, *Chem. Rev.* 2007, **107**, 1011; (c) K. Y. Pu, B. Liu, *Adv. Funct. Mater*. 2009, **19**, 277.

12 (a) Y. Q. Tian, C. Y. Chen, C. C. Yang, A. C. Young, S. H. Jang, W. C. Chen, *Chem. Mater*. 2008, **20**, 1977; (b) R. T. K. Kwok, J. L. Geng, J. W. Y. Lam, E. G. Zhao, G. Wang, R. Y. Zhan, B. Liu, B. Z. Tang, *J. Mater. Chem. B* 2014, **2**, 4134.

13 (a) B. K. An, S. K. Kwon, S. D. Jung, S. Y. Park, *J. Am. Chem. Soc.* 2002, **124**, 14410; (b) J. Dong, J. W. Y. Lam, A. Qin, Z. Li, J. Sun, H. H. Y. Sung, B. Z. Tang, *Chem. Commun.* 2007, 40; (c) W. Z. Yuan, X. Y. Shen, H. J. Zhao, J. W. Y. Lam, L. Tang, B. Z. Tang, *J. Phys. Chem. C* 2010, **114**, 6090.

14 (a) M. Wang, G. X. Zhang, D. Q. Zhang, D. B. Zhu, B. Z. Tang, *J. Mater. Chem*. 2010, **20**, 1858; (c) J. Liang, R. T. K. Kwok, H. B. Shi, B. Z. Tang, B. Liu, *Appl. Mater. Interfaces* 2013, **5**, 8784.

15 (a) H. G. Lu, B. Xu, Y. J. Dong, F. P. Chen, Y. W. Li, Z. F. Li, J. T. He, H. Li W. J. Tian, *Langmuir*, 2010, **26**, 6838; (b) R. Martinez-Manez, F. Sancenon, *Chem. Rev*. 2003, **103**, 4419.

16 G. M. Sheldrick, SHELXTL V5.1 Software Reference Manual, Bruker AXS, Inc., Madison, Wisconsin, USA, 1997.

17 H. P. Zhou, Z. Zheng, G. Y. Xu, Z. P. Yu, X. F. Yang, L. H. Cheng, X. H. Tian, L. Kong, J. Y. Wu, Y. P. Tian, *Dyes Pigm*. 2012, 94, 570.

18 (a) H. G. Zhang, X. T. Tao, K. S. Chen, C. X. Yuan, S. N. Yan, M. H. Jiang, *Chinese Chem. Lett.* 2011, **22**, 647; (b) H. J. Lee, J. Sohn, J. S. Hwang, S. Y. Park, H. Choi, M. Cha, *Chem. Mater*. 2004, **16**, 456.

19 M. J. Frisch, G. W. Trucks, H. B. Schlegel, Gaussian 03 Gaussian, Inc.: Wallingford CT, 2004.

20 (a) B. Z. Tang, Y. H. Geng, J. W. Y. Lam, B. S. Li, *Chem. Mater*. 1999, **11**, 1581; (b) F. K. Wang, G. C. Bazan, *J. Am. Chem. Soc*. 2006, **128**, 15786; (c) Y. N. Hong, J. W. J. Lam, B. Z. Tang, *Chem. Commun*. 2009, 4332.

21 (a) S. Goswami, S. Das, K. Aich, *Tetrahedron Lett*. 2013, **54**, 4620; (b) M. H. Yang, P. Thirupahi, K. H. Lee, *Org. Lett*. 2011, **13**, 5028; (c) M. Shellaiah, Y. H. Wu, A. Singh, M. V. R. R, H. C. Lin, *J. Mater. Chem. A*. 2013, **1**, 1310.

22 H. A. Benesi, J. H. Hildebrand, *J. Am. Chem. Soc.* 1949, **71**, 2703.

23 (a) M. Shortreed, R. Kopelman, M. Kuhn, B. Hoyland, *Anal. Chem*. 1996, **68**, 1414; (b) J. P. Xu, Y. Fang, Z. G. Song, J. Mei, L. Jia, A. J. Qin, J. Z. Sun, J. Ji, B. Z. Tang, *Analyst* 2011, **136**, 2315.

24 (a) M. Q. Wang, K. Li, J. T. Hou, M. Y. Wu, Z. Huang, X. Q. Yu, *J. Org. Chem*. 2012, **77**, 8350; (b) N. Shao, Y. Zhang, S. M. Cheung, R. H. Yang, W. H. Chan, T. Mo, K. A. Li, F. Liu, *Anal. Chem*. 2005, **77**, 7294.

25 (a) M. D. Allendorf, C. A. Bauer, R. K. Rhakta, R. J. T. Houk, *Chem. Soc, Rev*. 2009, **38**, 1330; (b) N. Rendón, A. Bourdolle, P. L. Baldeck, H. L. Bozec, C. Andraud, S. Brasselet, C. Copéret, O. Maury, *Chem. Mater*. 2011, **23**, 3228; (c) F. X. Zhou, Z. Zheng, H. P. Zhou, W. Z. Ke, J. Q. Wang, Z. P. Yu, F. Jin, J. X. Yang, J. Y. Wu, Y. P. Tian, *CrystEngComm*. 2012, **14**, 5613.

26 (a) H. S. Jung, P. S. Kwon, J. W. Lee, J. I. Kim, C. S. Hong, J. W. Kim, S. Yan, J. Y. Lee, J. H. Lee, T. Joo, J. S. Kim, *J. Am. Chem. Soc*. 2009, **131**, 2008; (b) A. Mallick, M. C. Mandal, B. Haldar, A. Chakrabarty, P. Das, N. Chattopadhyay, *J. Am. Chem. Soc*. 2006, **128**, 3126; (c) D. T. Quang, J. S. Kin, *Chem. Rev*. 2010, **110**, 6280.

27 (a) H. Y. Li, X. Q. Zhang, Z. G. Chi, B. J. Xu, W. Zhou, S. W. Liu, Y. Zhang, J. R. Xu, *Org. Lett*. 2011, **13**, 556; (b); (c) X. Q. Zhang, Z. G. Chi, J. Y. Zhang, H. Y. Li, B. J. Xu, X. F. Li, S. W. Liu, Y. Zhang, J. R. Xu, *J. Phys. Chem. B* 2011, **115**, 7606; (c) M. J. Teng, X. R. Jia, S. Yang, X. F. Chen, Y. Wei, *Adv. Mater.* 2012, **24**, 1255; (d) J. W. Chung, Y. You, H. S. Huh, B. K. An, S. J. Yoon, *J. Am. Chem. Soc*. 2009, **131**, 8163.

28 M. D. Yang, D. L. Xu, W. G. Xi, L. K. Wang, J. Zheng, J. Huang, J. Y. Zhang, H. P. Zhou, J. Y. Wu, Y. P. Tian, *J. Org. Chem*. 2013, **78**, 10344.